Vol 13 No 12, December 2004
1009-1963/2004/13(12)/1992-07

Chinese Physics

© 2004 Chin. Phys. Soc.
and IOP Publishing Ltd

Application of the high-resolution Godunov method to the multi-fluid flow calculations*

Bai Jing-Song(柏劲松)†, Li Ping(李 平), Zhang Zhan-Ji(张展冀),
Hua Jing-Song(华劲松), and Tan Hua(谭 华)

Institute of Fluid Physics, China Academy of Engineer Physics, Mianyang 621900, *China*

(Received 2 March 2004; revised manuscript received 1 July 2004)

In this paper, we have numerically solved the multi-fluid problems using an operator-split two-step high-resolution Godunov PPM (parabolic piecewise method) for the flow in complex geometries. By using the front capturing method, the PPM integrator captures the interface in the solution process. The basic multi-fluid integrator is coupled to a Cartesian grid algorithm where a VOF (volume of fluid) representation of the fluid interface is also used. As an application of this method, we test the 2D interfacial advection example and simulate an experimental hypervelocity launcher model from Sandia National Laboratories. The computational design of the hypervelocity launcher is also given in the paper.

Keywords: high resolution, PPM, multi-fluid, VOF
PACC: 0270, 0340G, 0660J

1. Introduction

A main difficulty for simulating compressible multi-fluid flow is the treatment of moving material interfaces and their vicinity. In general, there are two basic approaches to the treatment of such contact discontinuities. The first approach is front tracking, as developed by Glimm *et al.*[1] In the front tracking, accurate boundary conditions can be imposed on the moving interfaces and the contact discontinuities are treated as the internal moving boundary. However, a front tracking approach is usually complicated if it is wished to treat large interfacial deformation. At times reconstruction of the tracked interface is required.[2,3] Another disadvantage arising from the use of front tracking is the possible numerical instability caused by the presence of extremely small grid size. The second approach is front capturing, which represents contact discontinuities as steep gradients to be resolved over a few grid cells. A main advantage of employing front capturing is its relative simplicity and easy extension to multi-dimensions. What are used to obtain the flow field are normally high-resolution schemes like TVD, ENO, WENO, lattice-BGK[4] in order to handle the possible shock wave. When such a scheme is employed to solve multi-fluid flow, however, numerical inaccuracies and oscillations can occur at the interfaces. Various techniques have been developed to overcome these difficulties.[5–11] A good summary may be found in Ref.[12]. The VOF (volume of fraction) method is a popular and successful technique to capture interfaces in both multi-fluid and free-surface flows. It is based on a characteristic function Y with a value of 1 in one fluid and 0 in the other fluid or vacuum. In this paper, we describe an algorithm for inviscid compressible multi-fluid flows contained in complex geometries respectively with one, two and three space dimensions. The basic algorithm is an operator split two-step three-order Godunov PPM method used to solve the Euler equations for multi-fluid flow. The first step is the Lagrange step in which the computation cells are distorted to follow the material motion, and the second step is the Remap step where the distorted cells are mapped back onto the Euler meshes. The algorithm captures, but does not track, the interfaces between distinct materials while maintaining a VOF representation of the constituent materials.

2. Computational method

*Project supported by the Foundation of China Academy of Engineering Physics (Gtant No 20040650).
†E-mail: bjsong_mail@21cn.com

2.1. Basic equations

In this paper, we apply a spatial operator-split scheme to solve the multi-dimensional problems. So, we mainly discuss the 1D (i.e. x-sweep) PPM for a multi-material system. Based on the VOF of the fluid model, we combine the PPM with interface tracking to solve the Euler hydrodynamic equations, which is referred to as a two-step Lagrange/Remap algorithm of solving multi-fluid problems. The first step is the Lagrange step in which the computation cells are distorted to follow the material motion, and the second step is the Remap step where the distorted cells are mapped back onto the Euler meshes. The Euler control equations can be written as

$$\begin{cases} \dfrac{\partial \rho}{\partial t} + \dfrac{\partial (\rho u)}{\partial x} = 0, \\ \dfrac{\partial (\rho u)}{\partial t} + \dfrac{\partial \left(\rho u^2 + p\right)}{\partial x} = 0, \\ \dfrac{\partial (\rho E)}{\partial t} + \dfrac{\partial \left[(\rho E + p)\, u\right]}{\partial x} = 0, \\ \dfrac{\partial Y^{(i)}}{\partial t} + u \dfrac{\partial Y^{(i)}}{\partial x} = 0, \quad i = 1, \ldots, N-1, \end{cases} \tag{1}$$

where ρ is the density, u is the velocity, p is the pressure, E is the total energy of a unit mass, N is the kind of materials and $Y^{(i)}$ is volume fraction of the ith material. In a mixed-cell containing N materials, the volume fractions satisfy $\sum_1^N Y^{(i)} = 1$. The total energy of a unit mass is given by

$$E = e + u^2/2, \tag{2}$$

where e is the specific energy. A simplified Gruneisen equation of state (EOS) is used in this paper

$$p = (\gamma - 1)\rho e + c_0^2(\rho - \rho_0), \tag{3}$$

where γ is the constant of material, ρ_0 and c_0 are the density and sound speed under the normality, respectively.

2.2. Multi-fluid PPM

To effectively capture interfaces of the materials, we apply a two-step Lagrange/Remap algorithm to solve Eq. (1). So, one time-step of calculation can be transformed into a four-step calculation: (1) the piecewise parabolic interpolation of physical quantities, (2) approximately solving Riemann problems, (3) evolution of the Lagrange equations and (4) mapping the physical quantities back onto the Euler meshes. In step (1), the piecewise parabolic interpolation of physical quantities is implemented according to Ref.[13]. In step (2), the Riemann problem is solved by using of the double shock wave approximately as seen in Ref.[14], which is just the equation of state in the same form as Eq.(3). We mainly discuss steps (3) and (4) here.

2.2.1. Lagrange step

The Lagrange equation for multi-fluid can be written as

$$\begin{cases} \dfrac{\partial \tau}{\partial t} - \dfrac{\partial (r^\alpha u)}{\partial m} = 0, \\ \dfrac{\partial u}{\partial t} + r^\alpha \dfrac{\partial p}{\partial m} = 0, \\ \dfrac{\partial E}{\partial t} + \dfrac{\partial (r^\alpha u p)}{\partial m} = 0, \\ \dfrac{\partial Y^{(i)}}{\partial t} = 0, \end{cases} \tag{4}$$

where τ is the specific volume, α is 0, 1, 2 respectively corresponding to plane, axial symmetry and spherical symmetry problems, r is the spatial coordinate, m is the mass: $m = \int_{r_0}^{r} \rho r^\alpha \mathrm{d}r$.

After the Lagrange step we can obtain the distribution of the physical quantities, $\left\{\tau_j^{n+1}\right\}$, $\left\{u_j^{n+1}\right\}$, $\left\{E_j^{n+1}\right\}$ and the positions of new grids $\left\{r_{j\pm1/2}^{n+1}\right\}$. Also, the pressure distribution $\left\{p_j^{n+1}\right\}$ can be given by the equation of state, and $\left\{\left(Y^{(i)}\right)_j^{n+1}\right\}$ will not be changed. The formulae are as follows:

$$\begin{cases} r_{j+1/2}^{n+1} = r_{j+1/2}^n + \tilde{u}_{j+1/2}\Delta t, \\ \tau_j^{n+1} = \dfrac{\left(r_{j+1/2}^{n+1}\right)^{\alpha+1} - \left(r_{j-1/2}^{n+1}\right)^{\alpha+1}}{(\alpha+1)\,\Delta m_j}, \\ u_j^{n+1} = u_j^n - \dfrac{1}{2}\dfrac{\Delta t}{\Delta m_j}\left(\sigma_{j+1/2} + \sigma_{j-1/2}\right)\left(\tilde{p}_{j+1/2} - \tilde{p}_{j-1/2}\right), \\ E_j^{n+1} = E_j^n - \dfrac{\Delta t}{\Delta m_j}\left(\sigma_{j+1/2}\tilde{u}_{j+1/2}\tilde{p}_{j+1/2} - \sigma_{j-1/2}\tilde{u}_{j-1/2}\tilde{p}_{j-1/2}\right), \end{cases} \tag{5}$$

$$\sigma_{j+1/2} = \frac{\left(r_{j+1/2}^{n+1}\right)^{\alpha+1} - \left(r_{j+1/2}^{n}\right)^{\alpha+1}}{(\alpha+1)\left(r_{j+1/2}^{n+1} - r_{j+1/2}^{n}\right)}, \tag{6}$$

where $\tilde{p}$ and $\tilde{u}$ are the pressure and velocity of Riemann solver at the grid interfaces, respectively.

2.2.2. Remap step

In the Lagrange step, the computation cells are distorted to follow the material motion, and in the Remap step, the distorted cells are mapped back onto the Euler meshes. The piecewise parabolic interpolation and integral methods in this step are the same as in the Lagrange step.

After the Remap step, the physical quantities in Euler meshes are defined as $(\rho_{\rm Euler})_j^{n+1}$, $(u_{\rm Euler})_j^{n+1}$, $(E_{\rm Euler})_j^{n+1}$, $\left(\left(Y^{(i)}\right)_{\rm Euler}\right)_j^{n+1}$, one fluid volume element through the grid boundary $j+1/2$ is defined as $\Delta V^*_{j+1/2}$ and the averages of physical quantities are defined as $\left(\rho^*, u^*, p^*, \left(Y^{(i)}\right)^*\right)_{j+1/2}$. The density in the Lagrange step is $\rho_j^{n+1} = 1/\tau_j^{n+1}$, therefore

$$\Delta m_j^{n+1} = \rho_j^{n+1} V_j^{n+1}, \tag{7}$$

$$\Delta m_j^n = (\rho_{\rm Euler})_j^n V_j^n, \tag{8}$$

$$\Delta m^*_{j+1/2} = \rho^*_{j+1/2} \Delta V^*_{j+1/2}, \tag{9}$$

$$\Delta E^*_{j+1/2} = \frac{1}{2}(u^*_{j+1/2})^2 \Delta m^*_{j+1/2} + \Delta e^*_{j+1/2}, \tag{10}$$

$$\begin{aligned}(\rho_{\rm Euler})_j^{n+1} =&[\Delta m_j^{n+1} - (\rho^*_{j+1/2}\Delta V^*_{j+1/2} \\ &- \rho^*_{j-1/2}\Delta V^*_{j-1/2})]/V_j^n,\end{aligned} \tag{11}$$

$$\begin{aligned}(u_{\rm Euler})_j^{n+1} =&[u_j^{n+1}\Delta m_j^{n+1} - (u^*_{j+1/2}\Delta m^*_{j+1/2} \\ &- u^*_{j-1/2}\Delta m^*_{j-1/2})]/\Delta m_j^n,\end{aligned} \tag{12}$$

$$\begin{aligned}((Y^{(i)})_{\rm Euler})_j^{n+1} =&[(Y^{(i)})_j^{n+1} V_j^{n+1} \\ &- ((Y^{(i)})^*_{j+1/2}\Delta V^*_{j+1/2} \\ &- (Y^{(i)})^*_{j-1/2}\Delta V^*_{j-1/2})]/V_j^n,\end{aligned} \tag{13}$$

$$\begin{aligned}(E_{\rm Euler})_j^{n+1} =&[E_j^{n+1}\Delta m_j^{n+1} - (\Delta E^*_{j+1/2} \\ &- \Delta E^*_{j-1/2})]/\Delta m_j^n,\end{aligned} \tag{14}$$

where $\Delta e^*_{j+1/2}$ is the convection of specific energy through the grid boundary $j+1/2$. We can extend the process to 2D and 3D cases by using the spatial operator-split algorithm.

3. Examples

3.1. Accuracy of the multi-fluid problem

Example 1 We use 1D numerical calculation of the two different gases to test the accuracy of multi-fluid PPM. These two gases are described by an ideal gas EOS, $p = (\gamma - 1)\rho e$. The initial distribution is expressed with dimensionless parameters as

$$(\rho, u, p, \gamma, Y^{(1)}) = \begin{cases} (4, 0, 4, 1.2, 1.0) & x \le 0.5, \\ (1, 0, 1, 1.4, 0.0) & x > 0.5. \end{cases}$$

Two mesh sizes are used in our calculations, the coarser $h = 0.01$, and the finer $h = 0.005$ respectively. The calculations are in Table 1. It is obvious that the accuracy of volume of fraction is more than first order, and the maximal reaches 1.73.

Table 1. The max-norm error, 1-norm error and error constant of the density, momentum, total energy and volume fraction constants in Example 1.

Content		ρ	ρu	ρE	$Y^{(1)}$
$h = 0.01$	1-norm	0.193088×10^{-1}	0.150295×10^{-1}	0.119751	0.952918×10^{-2}
	Max-norm	0.191458	0.212033	0.192309×10^{1}	0.387095
$h = 0.005$	1-norm	0.499521×10^{-2}	0.375490×10^{-2}	0.313246×10^{-1}	0.287670×10^{-2}
	Max-norm	0.123884	0.837553×10^{-1}	0.938315	0.189567
Accuracy τ	1-norm	1.95	2.00	1.93	1.73
	Max-norm	0.63	1.34	1.04	1.03
Error constant C	1-norm	0.154×10^{3}	0.151×10^{3}	0.886×10^{3}	0.272×10^{2}
	Max-norm	0.345×10^{1}	0.102×10^{3}	0.226×10^{3}	0.444×10^{2}

3.2. Test of the 2D interfacial advection along with 45 degree

Example 2: A copper cylinder with a diameter 0.01m and a copper cuboid with each side of 0.01m both move at a speed u=v=10km/s along a direction at 45 degree in the air. The region of calculation is $[0, 0.1\text{m}]\times[0, 0.1\text{m}]$, and the mesh grid is 200×200. Figure 1 shows the theoretical and numerical results of distribution of the volume fraction 0.1, 0.3, 0.5, 0.7 and 0.9 at t = 0.0, 2.0μs, 4.0μs, and 6.0μs, respectively. Figure 2 shows the theoretical and numerical results of distribution of the density at the time 6.0μs, the copper cuboid density is plotted at a section with y=0.085 and the copper cylinder density is plotted at

a section with y=0.07. Comparison between theoretical and numerical results for the volume fraction of the copper is given in Table 2. It is obvious that the relative error of cuboid is larger than that of cylinder in our calculations.

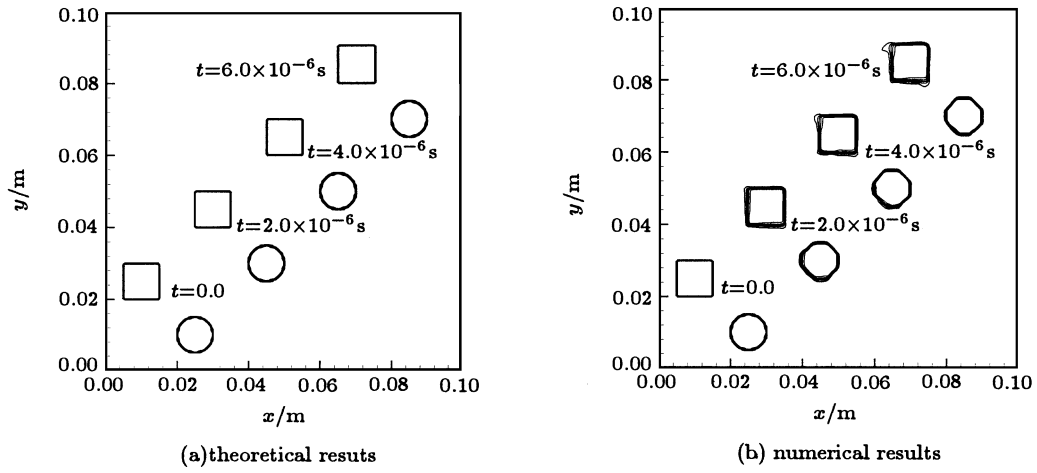


Fig.1. 2D interfacial advection moving at 45 degree.

Table 2. Comparison between theoretic and numerical results of the volume of fluid.

Shape	t/μs	Theoretical/m^2	Numerical/m^2	Relative error/%
Cylindrical	0.0	7.8539×10^{-5}	7.8393×10^{-5}	0.1859
	2.0		8.0185×10^{-5}	2.0958
	4.0		8.0359×10^{-5}	2.3173
	6.0		8.0644×10^{-5}	2.6802
Box	0.0	1.0000×10^{-4}	1.0000×10^{-4}	0.0000
	2.0		1.0630×10^{-4}	6.3000
	4.0		1.0741×10^{-4}	7.4100
	6.0		1.0927×10^{-4}	9.2700

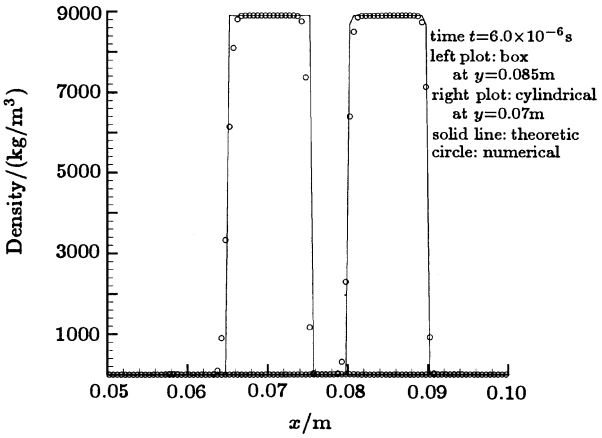


Fig.2. Comparison between theoretical and numerical results of the density distribution at the time 6.0μs.

3.3. Computation based on the Sandia hypervelocity experimental model

Example 3: This example comes from Ref.[15]. The experimental impactor configuration is indicated in Fig.3. The two-stage light-gas gun used in these studies had a bore diameter of 29mm. As indicated in this figure, a two-stage light-gas gun projectile facing a graded-density impactor is made to impact a thin flier plate located at the muzzle end of the barrel. The graded-density impactor consisted of six layered materials. They are TPX plastic, magnesium, aluminium, titanium, copper and tantalum and arranged in the order of impedance from low to high values. The flier plate materials used in this study were titanium (Ti-6-Al-4V) and aluminium. As indicated in Fig.3, a TPX plastic buffer was used in this experiment. We select three experimental models to perform the calculation by using the MFPPM and compare them with those experimental results. Table 3 shows the thickness of each material, the initial velocity of the graded-density impactor, Sandia's experimental results and the calculations by using MFPPM in this work. The axial velocity history of the flier plates from MFPPM is indicated in Fig.4. Compared to the Sandia experimental results, the relative error of the axial velocity

from MFPPM is 0.67%. Positions of the interfaces at 1.0μs and 2.0μs are plotted in Fig.5.

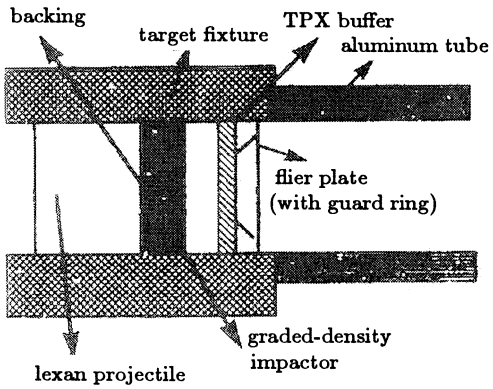


Fig.3. Schematic of a graded-density.

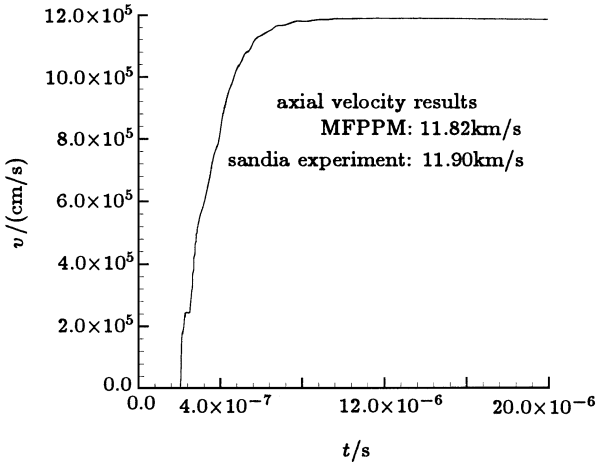


Fig.4. Axial velocity curves of the flyer-plate.

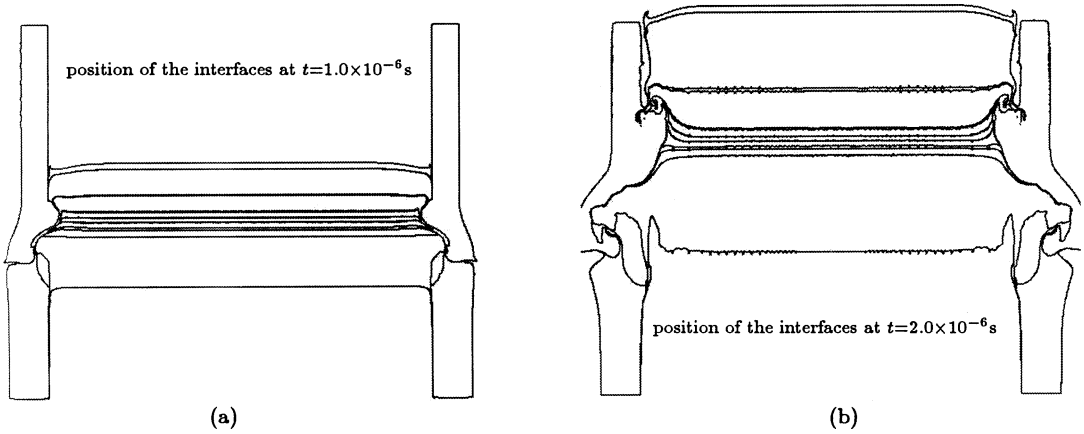


Fig.5. Positions of the interfaces at 1.0μs and 2.0μs.

Table 3. Comparison between the flier plate velocities obtained respectively from Sandia experiment and numerical calculation using MFPPM.

Experiment No.	Multi-Ply Assembly by Thickness/mm	Buffer/Flier-Plate Thickness/mm	Impact Velocity/(km/s)	Flier-Plate Material/ Velocity/(km/s)	MFPPM Velocity Result/(km/s)
EHVL2	0.61/0.30/0.24/0.32/0.20/0.44	1.21/0.43	7.35	Ti6/11.9	11.82

3.4. Computational design of hypervelocity launcher

Example 4: This is a design model for hypervelocity launch, and the schematic of the configuration is indicated in Fig.6(a). The graded-density impactor consists of seven layered materials: titanium, tungsten, copper, titanium, aluminium, magnesium–aluminium alloy and lexan. The thickness/diameter of each material is 0.5mm/38mm, 2.0mm/20.4mm, 0.3mm/20.4mm, 0.4mm/20.4mm, 0.5mm/20.4mm, 0.6mm/20.4mm and 2.0mm/20.4mm, respectively. The layered impactor velocity for the design model initially is 6.0km/s. The flier plate with a thickness/diameter of 2.0mm/16mm is of titanium, the buffer layer material is lexan with a thickness/diameter of 2.9mm/38mm and the barrel material is tungsten alloy.

We present the interfacial positions of the materials at t = 1.0μs, 3.0μs, 5.5μs in Figs.6(b), (c) and (d). The axial velocities and pressure histories at the quarter, center and three-quarter points are plotted in Fig.7. The average velocity of the flyer plate is about 10.2km/s, and the maximal pressure at the position of the quarter is about 76.6GPa. It is obvious that

the velocity has a jump (weak shockness) at the beginning, then increases slowly, and finally achieves an almost stable state. After 3.0μs, the pressure of the flier plate is almost zero (nearly shockless) and the flier plate remains flight attitude well, but for small distortions.

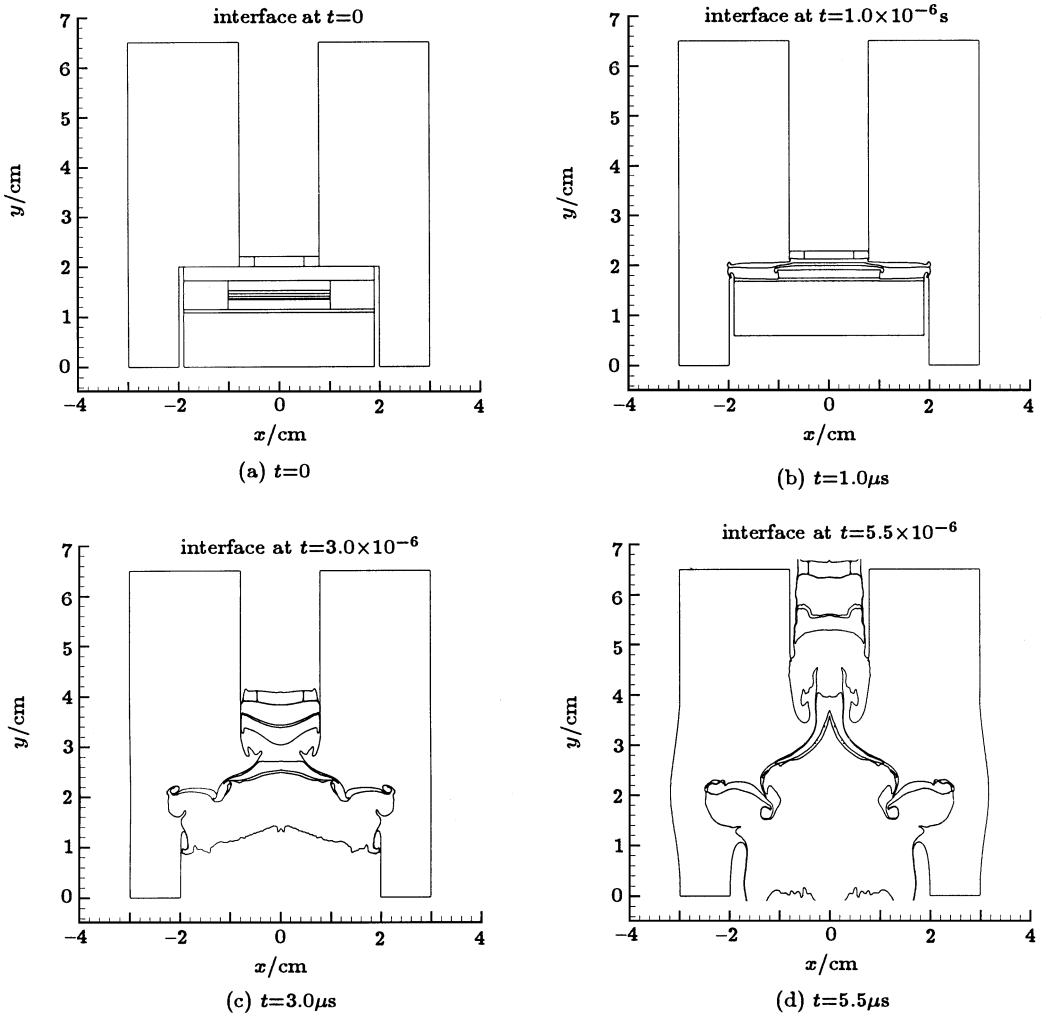


Fig.6. Configurations of the interfaces.

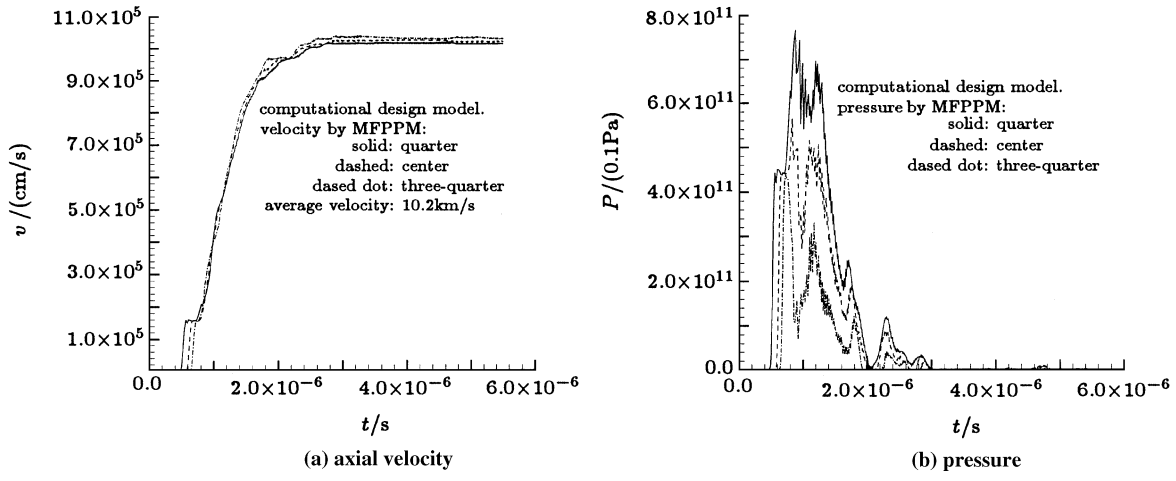


Fig.7. Axial velocities and pressures of the flyer-plater at quarter, center and three-quarter points.

4. Conclusion

Based on multi-fluid VOF and PPM, we have presented a high-resolution numerical calculation method to simulate the multi-fluid flows. As an application of this method, we simulate the experimental hypervelocity launchers of Sandia National Laboratories, and obtain the numerical results consistent with those experimental results. Also, we have tested the front capturing method for the interfaces and applied it to the design of hypervelocity launcher successfully. Finally, we mention that the equation of state used in our method needs to be extended more generally in the future.

References

[1] Glimm J, Grove J W, Li X L, Shyue K M, Zeng Y and Zhang Q 1998 *SIAM J. Sci. Comput.* **19** 703

[2] Lafaurie B, Nardone C, Scardovelli R, Zaleski S and Zanetti G 1994 *J. Comput. Phys.* **113** 134

[3] Zhang Y, Yeo K S, Khoo B C and Wang C 2001 *J. Comput. Phys.* **166** 336

[4] Guo W B, Wang N C, Shi B C and Guo Z L 2003 *Chin. Phys.* **12** 67

[5] Larrouturou B 1991 *J. Comput. Phys.* **95** 31

[6] Karni S 1994 *J. Comput. Phys.* **112** 31

[7] Abgrall R 1996 *J. Comput. Phys.* **125** 150

[8] Jenny P, Muller B and Thomann H 1997 *J. Comput. Phys.* **132** 91

[9] Zhang Z and Chen L R 2003 *Chin. Phys.* **12** 79

[10] Xu Y S, Wu F M, Chen Y Y and Xu X Z 2003 *Chin. Phys.* **12** 621

[11] Cocchi J P and Sislian R 1997 *J. Comput. Phys.* **137** 265

[12] Abgrall R and Karni S 2001 *J. Comput. Phys.* **169** 594

[13] Colella P and Woodward P 1984 *J. Comput. Phys.* **54** 174

[14] Shyue K M 1998 *J. Comput. Phys.* **142** 208

[15] Chhabilads L C 1993 SAND-91-2816C, DE93 002467